TURBULENT PIPE FLOW WITH NON-UNIFORM BODY FORCE

Kui He[1], Shuisheng He[2], Mehdi Seddighi[3]

Department of Mechanical Engineering
University of Sheffield
Sheffield S1 3JD, UK

[1]Email:mep11kh@sheffield.ac.uk
[2]Email:s.he@sheffield.ac.uk (corresponding author)
[3]Email:seddighi@sheffield.ac.uk

ABSTRACT

We report an investigation into the effect of some typified non-uniform body forces on turbulence, which represents the key source of the 'abnormity' of many non-equilibrium turbulent flows, especially in mixed convection systems. It is shown that such forces may enhance or suppress turbulence in a way that is observed in many 'real' flows, including for example, temporally or spatially accelerated flows; boundary layer flow with adverse pressure; and flow in a heated tube. Flow statistics and structures generated from DNS are used to demonstrate the commonality of turbulence suppression in various flows.

INTRODUCTION

An interesting and extensively studied phenomenon in mixed convective heat transfer is the heat transfer enhancement and impairment due to the presence of buoyancy. The main reason is that turbulence can be suppressed or enhanced in such flows. The mechanism is often very complicated. However, it is well established that the direct effect of buoyancy (as a body force) causing the mean flow to distort, and then modifying turbulence production is an important phenomenon. This is the dominant mechanism for the flow 'irregularity' in most mixed convection problems encountered in a vertical tube.

Similarly, turbulence production may be suppressed or enhanced in many other situations such as accelerating/decelerating channel flows or a boundary layer flow subject to a favourable or adverse pressure gradient. Interestingly, flow acceleration and the pressure gradient can be seen as a 'body force' and in this way, the flow behaviour under the influence of the 'body force' can be studied in a more unified way.

We follow the above idea and focus on the effects of some carefully specified non-uniform body forces in a turbulent pipe flow. Direct numerical simulation (DNS) is employed in the investigations.

METHODOLOGY

The present study is based on a fully developed pipe flow with a radially non-uniformly distributed streamwise body force. Consequently, the governing equations read:

$$\nabla \cdot u = 0 \tag{1}$$

$$\frac{\partial u}{\partial t} + u \cdot \nabla u = -\nabla p + \frac{1}{Re}\nabla^2 u + f \tag{2}$$

where $f=(bf,\ 0,\ 0)$, which is defined in the following form:

$$bf = \begin{cases} 0 & r < r_0 \\ f_0\left(1 - \frac{R-r}{R-r_0}\right) r & r \geq r_0 \end{cases} \tag{3}$$

where r is radial coordinate and f_0 is maximum body force density. The equations are non-dimensionalised by the pipe radius R, the centreline streamwise velocity of the laminar Poiseulle flow of the 'base' case U_{p0} and density of the fluid ρ. The fluxes, namely, $q_z=u_z$, $q_r=ru_r$, $q_\theta=ru_\theta$, are introduced to circumvent the singularity on the axis of the pipe (Orlandi, 2001). The code has been validated against Fukagata and Kasagi's (1996) benchmark data (not shown). A radially non-uniform body force (bf, normalized by ρU_{p0}^2) is added at the right hand side of the streamwise momentum equation (eq.2) throughout the simulation, while the mass flow rate is kept at a constant. The amplitude of the body force is determined by integration of the body force over the flow domain (*intbf*). It is defined as

$$intbf = \iiint rbf d\theta dr dx \tag{4}$$

The *intbf** is *intbf* normalized by $\tau_{w0}\pi DL$, where τ_{w0}, D, and L are, respectively, the shear stress, diameter and the length of pipe. Two series of cases are studied. Group A contains a linearly distributed force with fixed maximum body force density but varying radial coverages (Fig. 1a). Group B comprises cases of a linearly distributed body force with fixed radial coverage but varying maximum density (Fig. 1b). These cases are used to study the effects of amplitude and coverage, which can be linked to the buoyancy parameter and density distribution (McEligot and Jackson, 2004; Bae, 2006) in real flow. The Reynolds number based on the bulk velocity and diameter is 5300. The corresponding Re_τ is ~180 for the reference or base case. 'Real' body forces in mixed convection cases (which involves the buoyancy force, ρg) and accelerating flows (in which the inertia, $\rho\ \partial U/\partial t$, is involved) or many other 'non-equilibrium' turbulent flows can often be represented by one of the above, or a combination of them, or with a slight variation.

1

RESULTS AND DISCUSSION

General features of the body force effect

Ensemble statistics are obtained by averaging in streamwise and spanwise directions, and then over 20 instantaneous flow fields with interval of $\Delta t=10$ after the flow is fully developed. Fig. 1 shows the distributions of body force in all cases. In cases A1~A4, the maximum body force density (f_0) next to the wall is fixed, but the extent to which the body force covers increases from $y^{+0}=15$ to 90 (y normalized by u_τ of the base flow, Fig. 1a), while, in cases B1~B6, the maximum body force density (f_0) increases from 0.0055 to 0.069, keeping the covering region within $y^{+0}=60$.
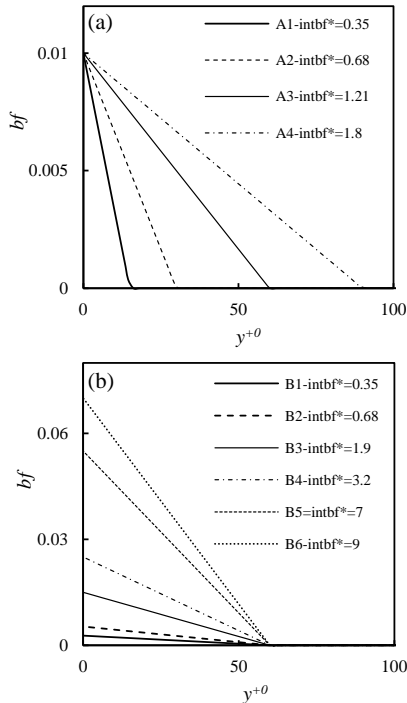

Figure 1. Body force distribution
(a) Group A; (b) Group B

The integrated body forces increase with the increase of the covering region or the body force density amplitude, which leads to steeper velocity profiles near the wall and a lower velocity in the centre. Fig.2 shows the profiles of mean velocities and Reynolds stress. 'Base' refers to the case, in which no non-uniform body force is applied. The flows of A1, A2, B1 and B2 show slight deviation from the velocity profile of the base flow. An 'M-shaped' velocity profile is eventually formed with the increase of the body force strength (e.g., A3, A4, B3, B4, B5, B6). The Reynolds shear stress also changes significantly (Figs. 2b&c). With the increase of the strength of the body force, the flow exhibits four different regimes: (i) slightly re-laminarisation (or turbulence-suppression) regime: turbulence is suppressed but does not completely disappear. With the increase of the strength of the body force, the reduction in turbulence is strengthened; (ii) 'complete' re-laminarisation regime: under such a condition, turbulence is very low and the flow is largely laminar; (iii) the slightly recovery regime: with further increase in the body force, the mean velocity

would take an 'M-shape' profile, and turbulence is re-generated, but only slightly in the centre region; (iv) strongly recovering regime: with the increase of the body force further, the turbulence is at a high rate both in the core and near wall region. The turbulent shear stress is however negative in the centre of the pipe. According to this classification (see Fig. 2c), A1, A2, B1 and B2 are slightly re-laminarised cases; A3, B3 are completely re-laminarised cases; A4 and B4 are slightly recovered cases; and B5, B6 are strong recovery cases.
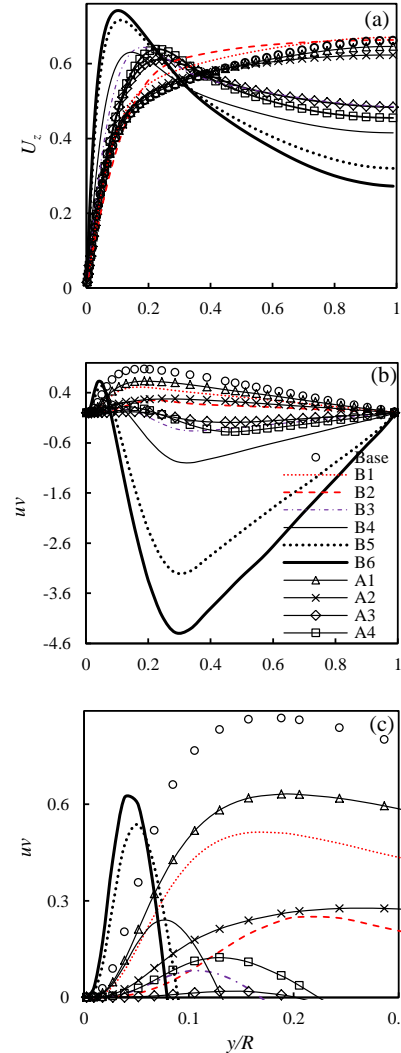

Figure 2. Mean velocity and turbulent shear stress; a) Mean velocity, b) turbulent shear

The detailed flow features of cases B1, B2, B3 and B6

In following, 4 typical cases are selected to be studied in detail, one from each regime. Fig. 3 shows the *r.m.s.* of streamwise and wall-normal fluctuating velocities. The *r.m.s.* velocities are reduced in the turbulence-suppression cases (B1, B2), with stronger reduction in the wall-normal component than in the streamwise direction (Fig. 3b). It is observed that case B3 shows a recovery but is mainly observed in the centre region. The streamwise *r.m.s.* velocity in all recovery cases shows two peaks. It is seen that the peak in the

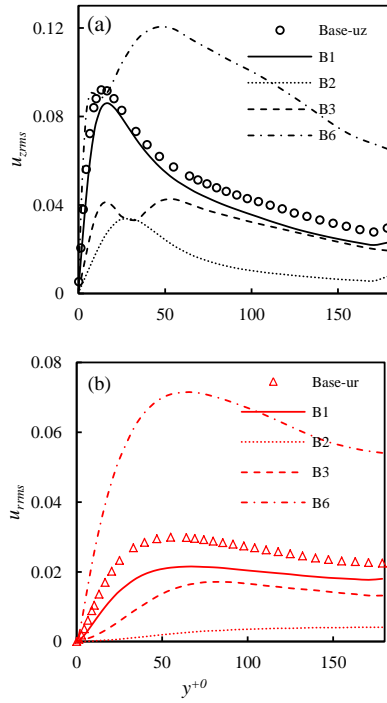central region of B6 is significantly higher than that in the base case.

Figure 3. u_{zrms} and u_{rrms} in B1, B2, B3 and B6

The budget terms are useful in terms of explaining these turbulence production behaviours. Figs. 4(a) &(b) show the radial distribution of budget terms of u_z' normalized with u_τ^4/ν for two selected cases (i.e., B1 & B6) together with the budget terms for the base case. The comparison illustrates the deviation of the budget distribution of B1 and B6 from that of an equilibrium steady flow. Case B1 shows a slight reduction in the production, turbulent transport, viscous diffusion, pressure strain and dissipation. The shear velocity is slightly reduced, therefore these reductions represent the absolute suppression of turbulence in the flow. The positions of the peak values for these terms move towards the centre of the pipe; this indicates that the near-wall structures are affected first. For B6, the production recovers, exhibiting two peaks. The production near the wall is similar to the typical shear flows resulting from the large velocity gradient in the wall region. In comparison, the peak production in the core region is due to a 'free' shear layer, resulting from the internal part of the M-shaped velocity profile. The peak production near the wall is closer to the wall in B6 than in B1. Unlike the near wall production, the production in the centre is mainly balanced by pressure strain and turbulent transport instead of dissipation and viscous diffusion. Interestingly, the pressure strain, which redistributes energy between the various components, recovers slightly but the distribution pattern is different from that of the base flow. There is a region between the wall turbulence and free shear layer turbulence where the pressure strain (PS) term is positive, indicating that the energy is transferred from wall normal and spanwise components to streamwise component. This is in contrast to the base flow in which the energy is
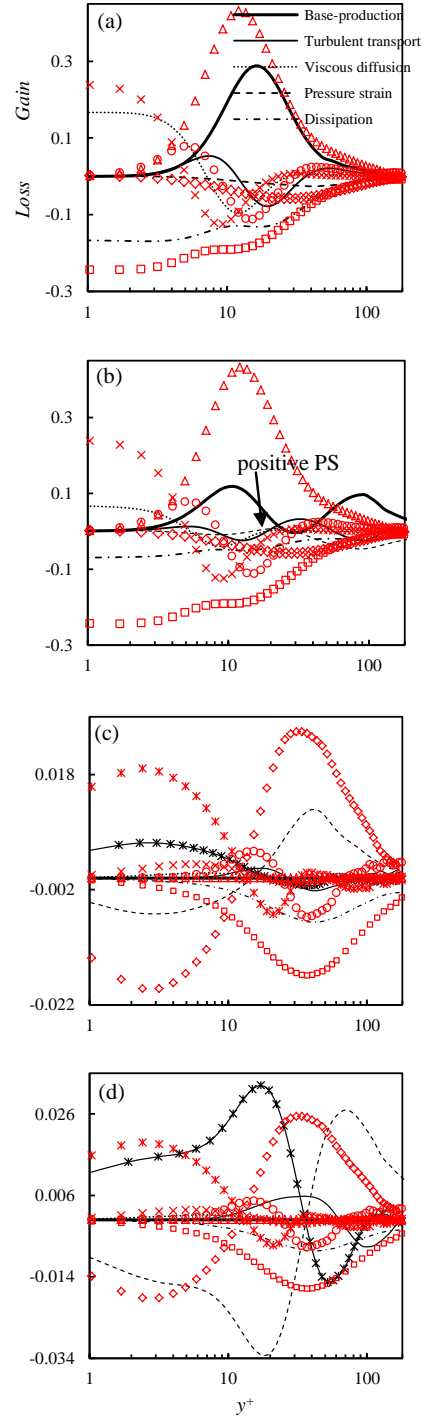

Figure 4. Budget terms of u_z' in selected cases. The base is shown in markers; other cases are shown with lines. triangular: production; diamond: pressure strain; star: pressure diffusion (star with line: coressponding term in base flow); cross: viscous diffusion; circle: turbulent transport; box: dissipation. (a) u_z budget of B1, (b) u_z budget of B6, (c) u_r budget of B1, (d) u_r budget of B6.

transferred from streamwise component to the other two components.

Figs. 4(c) &(d) show the budget terms of u_r'. The dominant terms are velocity pressure strain (pressure strain), velocity pressure diffusion (pressure diffusion) and dissipation in the base flow. The secondary dominant terms are turbulent transport and viscous diffusion. In the region $y^+<15$, the pressure strain is negative and is mainly balanced by pressure diffusion. In the other regions, pressure strain is positive and is mainly balanced by the dissipation. In case B1, the secondary terms disappear and the dominant terms are more strongly suppressed comparing to those in the u_z' budgets. In case B6, where the turbulence is strongly recovered, strong recoveries in pressure strain and pressure diffusion are seen. The turbulent transport term also recovers more notably than the viscous diffusion term. As it is shown in Fig.4(d), in the region $y^+<35$, the balance is established between pressure strain and pressure diffusion. However, the structure is changed in that the negative region of pressure strain is extended to $y^+=35$, whereas this term is positive beyond $y^+=12$ in base flow. In the region between $y^+=35$ and between $y^+=70$, the magnitude of pressure diffusion increases significantly, which can be neglected in the base flow. The pressure strain is mainly balanced by dissipation and pressure diffusion in this region.

The near wall flow structures of B1, B2, B3 and B6

Fig. 5 shows contour plots of streamwise fluctuation velocity for selected cases illustrating flow structures in the various regimes.
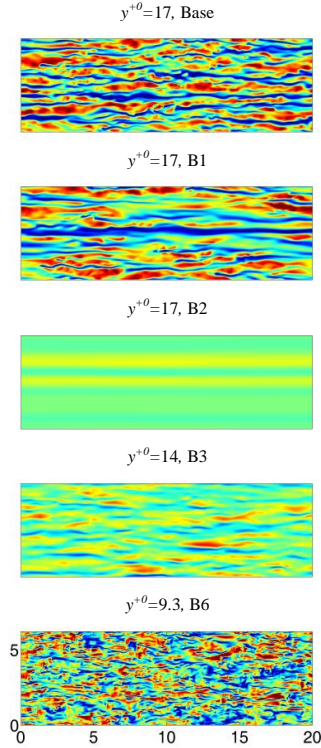
$y^{+0}=17$, Base

$y^{+0}=17$, B1

$y^{+0}=17$, B2

$y^{+0}=14$, B3

$y^{+0}=9.3$, B6

Figure 5. Flow structures in slected cases at $y^+ = 17$; Max:$2u_{zrms,p0}$, Min:$-2u_{zrms,p0}$.

For all selected cases, the y^+ (normalized with local u_τ) is fixed at 17, where typical shear flow structures can be observed. It is interesting to see that in the turbulence suppression case (B1), streaks are significantly strengthened and elongated compared to the base case. Case B2 is fully laminarized, and no near wall structures can be observed. The turbulence in B3 is recovering (but relatively weakly). The streaky structures are observed but these structures are shorter and weaker comparing to those of the base flow. The strongest recovered case B6 shows different structures to other cases. No clear streaky structures are identifiable.

The 3-D visaulization in fig. 6 shows the coherent structures near the wall, where case B2 is not included due to its completely laminaried state. The positive and negative values of u_z' are shown in green and blue colours, respectively. These rendered iso-surfaces are used to exhibit the streaky structures. The iso-surfaces in red colour are vortex structures which are visualized using λ_2 values (Jeong and Hussain, 1995). Here λ_2 is the second largest eigenvalue of the symmetric tensor $S^2 + \Omega^2$, where S and Ω are the symmetric and antisymmetric parts ofthe velocity gradient tensor, Δu. Only the lower half of the pipe is shown. Unlike the above contour plot, the reference value is the local peak value, which is better to show the near wall structures, especially in the case B6, where the turbulence is strongly recovered. Case B1 is interesting in that there are large low speed streaky structures but smaller high speed streaks in the flow. B3 is a recovered case, where the most obvious difference from the base flow is the increase in high speed strutures. This is also observed in the strongest recovered case B6. The near wall structure is not streaky and numerous high speed structures emergein this case, indicating that there is strong turbulence entraiment from the shear layer. These observations are consient with that from the contour plots.
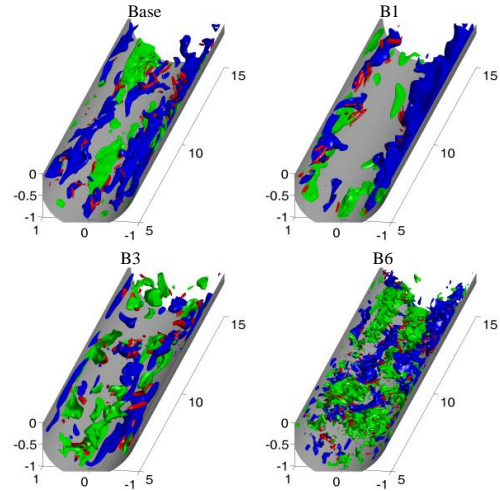

Figure 6.Vortical and streaky structures; u_z:$\pm1.3u_{zrms,p}$, λ_2:$-4\lambda_{2rms,p}$.

The Lumley trangule (Lumley, 1978) can be used to charaterize the flows. *II* and *III* are defined as

$$II = -\frac{1}{2}\left(b_{zz}^2 + b_{rr}^2 + b_{\theta\theta}^2 + 2b_{zr}^2\right) \qquad (5)$$

$$III = b_{\theta\theta}b_{zz}b_{rr} + b_{\theta\theta}b_{zr}^2 \qquad (6)$$

$$b_{ij} = \frac{\tau_{ij}}{\tau_{kk}} - \frac{1}{3}\delta_{ij} \qquad (7)$$

where, τ and δ are,respectively, the Reynolds stress and Kronecker delta function. Fig. 7 shows these parameters for all cases in group B. Case B1 is slighly laminarized, therefore the basical structure is still similar to that of the base flow, which is isotropic in the core region while the majority of the flow is rod-like. It is obvious to see the case B2 is compeletly laminarized and becomes 1-D turbulence in the near-wall region. As the turbulece recovers in B3, B4, B5, B6, it is shown that the core flows are turning into isotropic state. The near wall flow are shifting from the rod-like to disk-like flow.
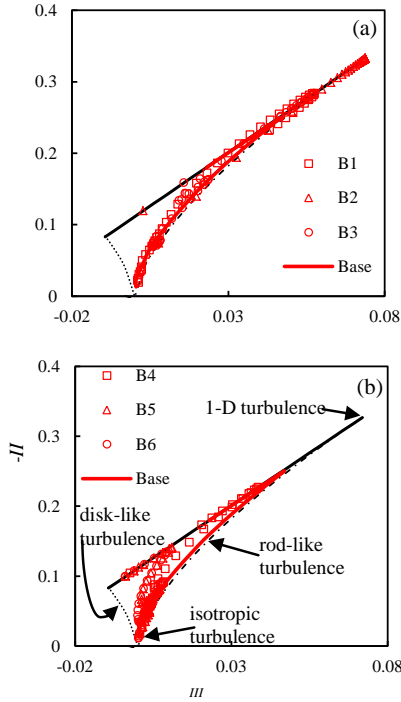

Figure 7. Lumley triangle of cases in Group B
(a) Base, B1, B2, B3 (b) Base, B4, B5, B6

The near wall flow activities of cases B1 and B6

The near wall flow activities, such as sweeps and ejections (Willmarth, 1972) are related to the near-wall coherent structures. The wall-normal motions are key ingredients in heat and mass transfer in wall bounded flows. Fig.8 shows the fractional contribution to Reynolds shear stress due to different turbulent events. In the base flow and case B1, the sweeps and ejections are the dominant events in the flow. They reduce in B1 and their distribution pattern changes, especially with the sweep events. The contribution of sweeps reduces more significantly from y^{+0}=15 to y^{+0}=42, comparing to other region. By contrast, this phenomenon is not observed in the contribution of ejections. In case B6, in the near-wall region, the Reynolds stress is still mainly contributed by the sweeps and ejections. However, the peak moves significantly towards the wall. The Q1 and Q3 are the dominant events in the outer layer, illustrating that the 'free' shear turbulence strongly interacts with the near-

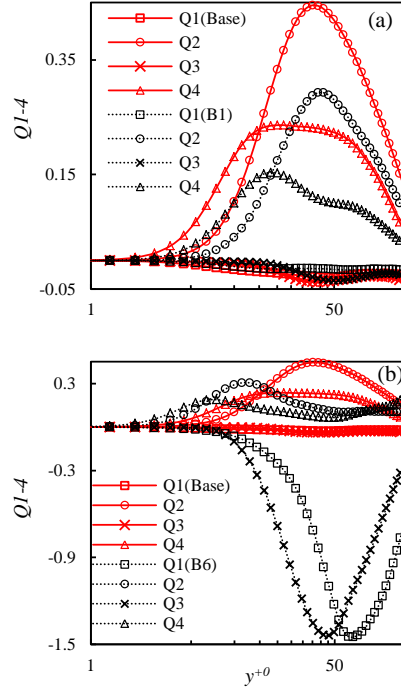wall turbulence. Fig. 9(a) &(b) show 3-D visualization of the sweeps and ejections of B1 and B6.

Figure 8. Fractional contribution to Reynolds shear stress (-uv>$Hu'v'$, with H=1) (a) B1; (b) B6
$Q1 = -\overline{u^+v^+}(u>0; v>0)$, $Q2 = -\overline{u^+v^+}$ ($u<0; v>0$),
$Q3 = -\overline{u^+v^+}$ ($u<0; v<0$), $Q4 = -\overline{u^+v^+}$ ($u>0; v<0$).

To identify these activities, isotropic surfaces of high Reynolds stress in near-wall region are plotted (only the flow activities between the wall and y^+=50 are visualized). The sweeps, ejections and the vortices are shown in blue, green and red colour, respectively. It is interesting to observe that, compared with the base flow, the ejections reduce, and the sweeps almost disappear in B1. The vortex structures are also reduced. In case B6, the Q2 and Q4 events in near-wall region are sponge-like flakes, while the vortex clusters are sponges of strings.
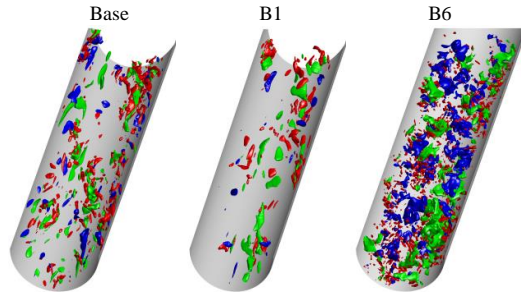

Figure 9. Sweeps and ejections in a) base, b) B1,and c) B6 cases; -uv> 0.6*max($u_{rms}v_{rms}$), λ_2=$\lambda_{2rms,max}$.

Correlations of different cases

It is clear from the results shown that both increasing the amplitude of the body force density and the region

where the body force is applied can increase the influence of the body force. The two means have very similar influence on the flow and turbulence. In fact, the extent to which the body force influence the flows largely depend on the amplitude of the integrated body force. The introduction of the body force can result in an increase or a decrease in friction depending on the balance of two competing effects, the reduction of turbulence which causes a reduction in friction and a more direct effect of the increased velocity gradient near the wall which causes an increase in the friction. Fig. 10(a) shows the correlation between the non-dimensionalized net force of friction and body force. This parameter measures the magnitude of the body force compared to the original shear. It is interesting to note that 'complete' laminarisation always occurs when the body force more or less balances the wall shear stress. The ratio between the integrated body force and friction of the base case ($\frac{\int r b f dr}{\tau_{w,0}}$) is, respectively, equal to 121% and 68% in A3 and B2, which are the two worst laminarized flow cases (see Fig.2). This trend is also reflected in other global parameters, such as the Reynolds number based on the momentum thickness, which is shown in fig.10(b).
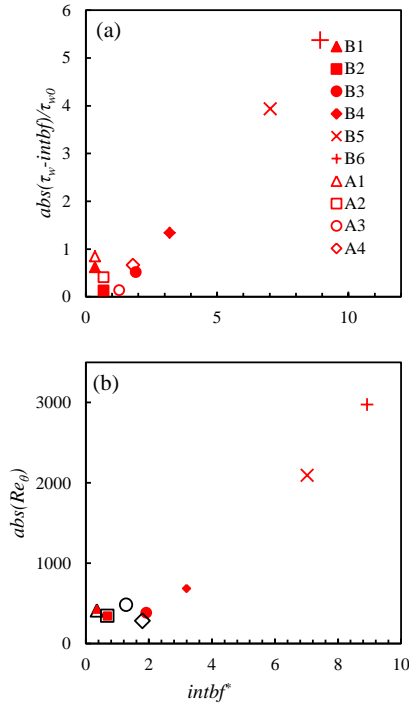

Figure 10. A correlation for all cases; body force against a) the net force friction, b) Re_θ.

CONCLUSIONS

It has been shown using DNS that a linearly-distributed body force can systematically cause flow re-laminarisation and turbulence re-generation (enhancement), depending on the strength of the body force. According to the state of the turbulence, a flow under the influence a distributed body force is classified into four groups, namely, the slightly laminarized flow,

'completely' laminarized flow, slightly recovered flow and strongly recovered flow. Each flow shows distinctive characteristics. For the slightly laminarized flow, the coherent structures near the wall are first suppressed, and sweeps and ejections events are both reduced but in different ways: the sweeps are reduced more significantly than the ejections. In the 'completely' laminarized flow, there is no wall normal turbulence but the streamwise component still remains in the flow. In a slightly recovered flow, the recovery of turbulence is limited to the 'free' shear layer region. Only in the strongly recovered flows, the near wall turbulence is also recovered. Their near wall part shows a similar budget and flow activity patterns to those of the base flow. These different types of flows can be correlated very well with some global parameters. It is shown by these correlation plots that a 'complete' laminarized flow case always coincides with a situation when the friction force largely balances the applied body force.

REFERENCE

Bae, J. H., Yoo, J. Y., Choi, H., and McEligot, D.M. 2006, "Effects of large density variation on strongly heated internal air flows", *Phys. Fluids,* 18, 075102-25.

Fukagata, F., and Kasagi, N. 2002, "Highly energy-conservative finite difference method for the cylindrical coordinate system", *J. Comput. Phys.*,181, 478.

Jeong, J., and Hussain, F. 1995, "On the identication of a vortex", *J. Fluid Mech.*, 285, 69-94.

Lumley, J. 1978, "Computational modelling of turbulent flows", *Adv.Appl.Mech.*, 18, 123-176.

McEligot,D.M., and Jackson, J.D. 2004, "Deterioration criteria for convective heat transfer in gas flow through non-circular ducts", *Nuclear Eng. and Des.,* 232, 327–333.

Orlandi, P. 2001, "Fluid Flow Phenomena: A Numerical Toolkit", Kluwer.

Willmarth, W.W., and Lu, S.S. 1972, "Structure of the Reynolds stress near the wall", *J. Fluid Mech.*,54, 65-92.